(Received 15 May 2025, Accepted 8 July 2025, Scheduled 21 July 2025)

Highly Sensitive Microstrip Patch Sensor for Water Salinity Monitoring

Hussein Jasim*, Amer Abbood Al-behadili, and Sadiq Ahmed

Electrical Engineering, College of Engineering, Mustansiriyah University, Baghdad 00964, Iraq

ABSTRACT: This paper presents the design and implementation of a microstrip patch sensor based on a single complementary split ring resonator (SC-SRR), operating at a resonant frequency of 2.44 GHz for salinity detection. The sensor evaluates liquid under test (LUT) by monitoring variations in resonant frequency, reflection coefficient, and quality factor to extract the complex permittivity. The proposed design was simulated using High Frequency Structure Simulator (HFSS) and fabricated on an FR-4 substrate, incorporating a Teflon container to prevent direct contact with the sensing surface. Simulated and measured results exhibit a significant agreement, validating the sensor's performance. A frequency shift of 104.4 MHz was observed as the salinity concentration varied from 0 to 100 parts per thousand, attributed to dielectric perturbation effects. The proposed sensor demonstrates several advantages, including non-contact and non-destructive measurement, reusability, cost-effectiveness, high sensitivity, minimal fluid volume requirement, and reliable accuracy. These features highlight its potential for applications requiring precise and efficient.

1. INTRODUCTION

Microstrip patch antennas (MPAs) are prevalent in sensing applications owing to their compact size, thin profile, light weight, affordability, durability, and sensitivity to variations in substrate dielectric properties [1]

Researchers have devised numerous microstrip designs, including U, S, C, hexagonal, and hexagonal with slot configurations, footprint for diverse uses [2–8]. Recent advancements in manufacturing technology and the emergence of printed circuits have enabled the progression of antenna-based sensors from fundamental ambient detection to advanced biomedical applications [9, 10]. Antennas used as sensors provide many advantages, such as the ability to acquire large amounts of high-quality data, being cost-effective, functioning without batteries, and requiring minimal maintenance. Microstrip is used in a variety of applications including measuring sugar and salt concentrations [11–13], and monitoring blood glucose levels [14–17]. From an environmental standpoint, sensors enable the detection of temperature [18, 19], humidity [20, 21], pH level [22]. The ingress of electromagnetic waves into a substance is significantly affected by frequency, with the range of 1–10 GHz being ideal for assessing variations in the dielectric characteristics of liquids [23, 24].

Environmental factors significantly influence the testing process; airborne dust particles affect signals and cause undesirable wave interference [25]; temperature fluctuations alter readings [26]; humidity affects radiation characteristics [27]; and two other crucial factors are the movement of the linked wires and sensor's stability.

Commonly employed indicators for achieving sensing functions include resonance frequency (f_r) shift-based sensing [28], reflection coefficient (S_{11}) [29], sensing utilizing both resonance frequency and return loss variation [30], and phase difference variation-based sensing [31].

Resonant sensors function based on the principle of resonance, capable of detecting physical and chemical alterations via variations in the resonant frequency. These sensors utilize the interaction between resonator structures and their surroundings, with the most prevalent types being split ring resonators (SRRs) [32], complementary split ring resonators (CSRRs) [33], single complementary split ring resonators (SC-SRRs) [34], multiple complementary split ring resonators (MCSRRs) [35], Hilbert structure [36], and Minkowski structure [37], wherein variations in resonant frequency correlate with alterations in the dielectric constant.

This article presents a highly sensitive microstrip patch sensor using single complementary split ring resonators (SC-SRRs) etched in the ground plane, proposed, designed, produced, and verified using 12 liquid samples, from fresh water to highly concentrated saline. The measured and simulated results exhibited remarkable concordance.

This manuscript has been organized as: 2. Microstrip patch sensor design, 3. Theoretical background, 4. Sensor performance, 5. Analytical simulation, 6. Creation of saline solutions and sensor fabrication, 7. Measurement and simulation results, 8. Sensitivity level comparison, 9. Comparison of the proposed sensor with existing works in the literature, and 10. Conclusion.

2. MICROSTRIP PATCH SENSOR DESIGN

A rectangular MPA with SC-SRR etched on the ground plane, operating at a resonance frequency of 2.44 GHz and using a 1.4 mm thick FR-4 substrate, is proposed, according to the spec-

* Corresponding author: Hussein Jasim (husseinj95@uomustansiriyah.edu.iq).

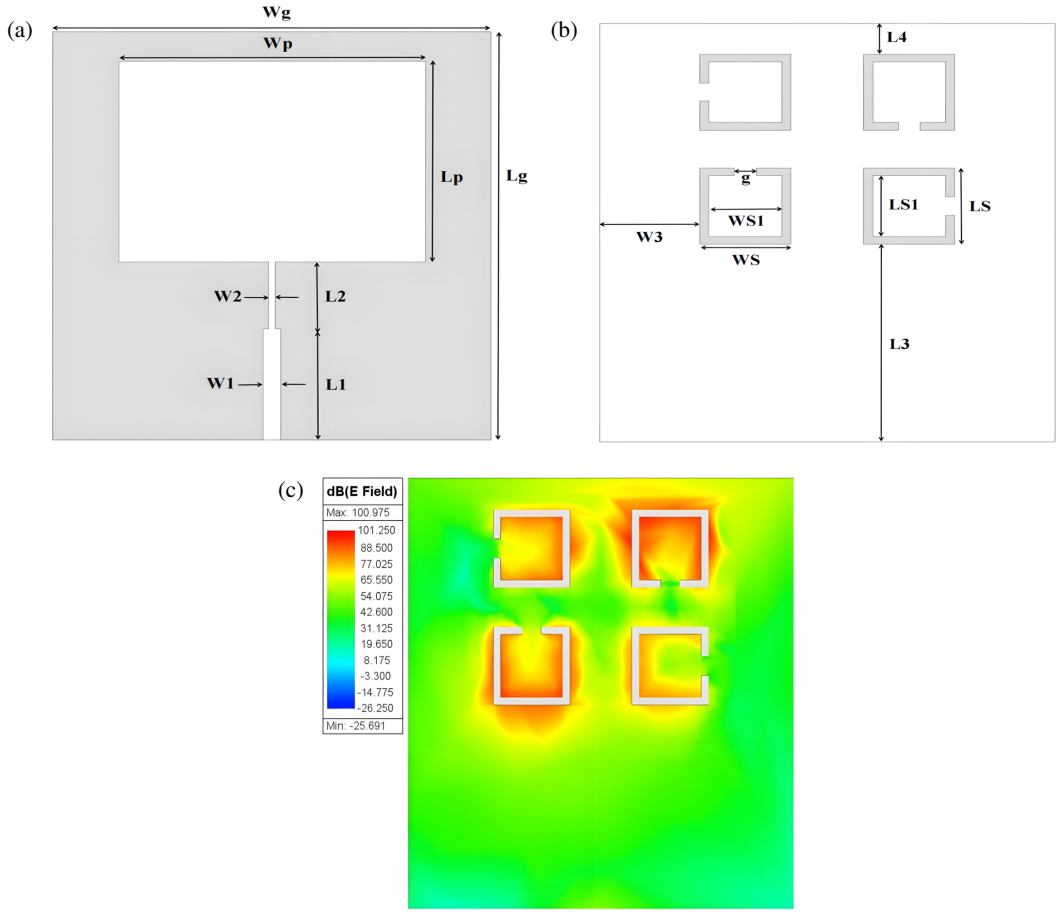

FIGURE 1. Proposed sensor configuration: (a) Top plane, (b) ground plane, and (c) simulated electric field distribution.

ified formulas [38].

$$Wp = \frac{C}{2f_r} \times \left(\frac{2}{\varepsilon_r + 1}\right)^{0.5} \quad (1)$$

$$\varepsilon_{eff} = \frac{\varepsilon_r + 1}{2} + \frac{\varepsilon_r - 1}{2} \times \left(1 + 12\frac{h}{Wp}\right)^{-0.5} \quad (2)$$

$$\Delta L = 0.412h\frac{\varepsilon_{eff} + 0.3}{\varepsilon_{eff} - 0.258} \times \frac{\frac{Wp}{h} + 0.264}{\frac{Wp}{h} + 0.8} \quad (3)$$

$$L_{eff} = \frac{C}{2f_r} \times \frac{1}{\sqrt{\varepsilon_{eff}}} \quad (4)$$

$$Lp = L_{eff} - 2\Delta L \quad (5)$$

where Wp denotes the patch width, C the speed of light at 3×10^8 m/s, ε_r the relative permittivity of substrate, h the substrate thickness, ε_{eff} the effective dielectric permittivity, ΔL the extension length attributable to the fringing field effect, L_{eff} the effective length, and Lp the patch length.

Four unique SC-SRRs etched on the ground plane were used in a particular arrangement to augment the electric field and improve sensitivity, as seen in Figure 1 and Table 1.

To avoid contact between the LUT and sensor, a container made of Teflon was selected based on appropriate criteria, such as its advantageous mechanical and electrical capabilities and non-absorption of liquids [39]. The Teflon exhibits a relative permittivity of 2.08 and a loss tangent of 0.001; the form and dimensions of the box are shown in Figure 2 and Table 2, respectively.

The purpose of the Teflon box is to prevent the liquid from contacting the sensor, as this can lead to the corrosion of critical sensor components, especially when using saline solutions as LUT.

TABLE 1. Dimensions of proposed sensor.

Parameters	Value (mm)	Parameters	Value (mm)
Wp	35	$W3$	11
Lp	27	WS	10
Wg	50	$WS1$	8
Lg	55	LS	10
$L1$	15	$LS1$	8
$L2$	9	$L3$	26
$W1$	2	$L4$	4
$W2$	0.78	g	2.5

TABLE 2. Dimensions of Teflon box.

Parameters	Value (mm)
Wb	35
$Wb1$	33.3
Lb	27
$Lb1$	25.3
hb	8
$hb1$	7

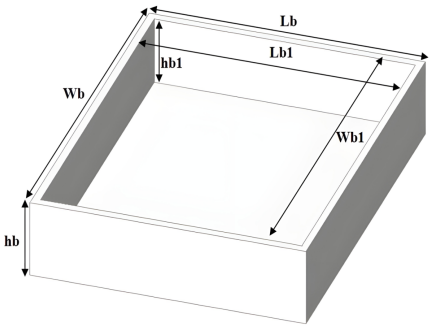

FIGURE 2. A Teflon box used as a container for liquid under test (LUT).

3. THEORETICAL BACKGROUND

3.1. Permittivity

The dielectric qualities of a material can be characterized by its complex permittivity [40]:

$$\varepsilon_r = \varepsilon_r' - j\varepsilon_r'' \tag{6}$$

It quantifies the extent to which a material is influenced by an electric field. The real component of permittivity or dielectric constant (ε_r') quantifies the extent to which energy from an external electric field is retained within a material. The imaginary component of permittivity, or dielectric loss factor (ε_r''), assesses the dissipative or lossy properties of a material when being subjected to an external electric field; the loss factor encompasses the influences of both dielectric loss and conductivity [41].

3.2. Dielectric Behavior of Saline Water

The polarization of H_2O molecules in water is seen in Figure 3. The molecular structure results in an asymmetrical charge distribution. In the absence of an external electric field, the molecules exhibit random orientations as depicted in Figure 3(b). When a field is applied, the molecules align such that their negative poles orient towards the positive voltage as depicted in Figure 3(c).

The molecules consequently produce a secondary electric field that counteracts the direction of the applied field. The outcome is that within the dielectric substance, the net electric field is diminished in magnitude [42]. The electric field stored within a material is referred to as the relative dielectric constant (ε_r'). The dielectric constant of a material directly affects the capacitance according to relation (7)

$$C = \frac{\varepsilon_r \varepsilon_o A}{d} \tag{7}$$

where C is the capacitance, ε_r the relative permittivity of the medium, and ε_o the free space permittivity (8.85×10^{-12} F/m), while area and displacement of plane are represented by A and d, respectively.

This formula demonstrates that an increase in the dielectric constant results in a corresponding increase in capacitance; a higher dielectric constant contributes to greater energy storage potential. On the other hand, dissolving salt in water leads to the formation of dissolved ionic compounds that enhance conductivity (σ), see Figure 4.

In order to demonstrate that elevating the salt concentration results in enhanced conductivity, we performed a straightforward experiment by utilizing a small red LED lamp, a 470 Ω resistor (to safeguard the lamp), a 9 V battery, a breadboard (to eliminate the need for soldering), and connecting wires. Figure 4(b) illustrates that the lamp exhibits significant luminescence at a concentration of 100 ppt, in contrast to Figure 4(a), where the light displays minimal illumination in freshwater.

4. SENSOR PERFORMANCE

The performance of the proposed sensor is evaluated by simulation in HFSS, and the electric field is mostly concentrated inside the individual rings. Therefore, for optimal sensitivity, the LUT should be placed in this region. To prevent direct contact between the liquid and sensor, it is necessary to use a vessel that acts as a container to hold the liquid samples. Figure 5 shows the final design of the proposed sensor and the magnitude of both the resonant frequency and reflection coefficient.

The results in Figure 6(a) are accomplished by changing ε_r' from 81 to 45, and σ is held constant at 0.001 S/m, while those in Figure 6(b) are accomplished by varying the parameter σ from 0.001 S/m to 12 S/m for each ε_r'.

Figure 6 illustrates that f_r, S_{11}, and Q fluctuate with changes in the dielectric constant and conductivity.

5. ANALYTICAL SIMULATION

Mixing salt with fresh water in varying amounts results in an elevation in the water's conductivity, as higher salt concentrations correspond to larger σ. It is evident that salt water exhibits greater conductivity than fresh water owing to the existence of dissolved ions in the solution, see Figure 4.

So it is essential to establish a numerical expression for conductivity. The Origin software was used to get the conductivity expression from the variation of the S_{11} at various concentrations.

$$\sigma = 495.89 \times \exp(-0.439 \times (-S_{11})) \tag{8}$$

Figure 7 displays the extracted S_{11} from the simulation data (see Figure 6(b)) accompanied by the conductivity for different dielectric constants. The correlation between S_{11} magnitude and σ is exponential, exhibiting a pronounced rise in curve steepness with rising salt concentrations, but ε_r' exhibits little variation across various conductivity levels; all of this is mathematically explained in (8).

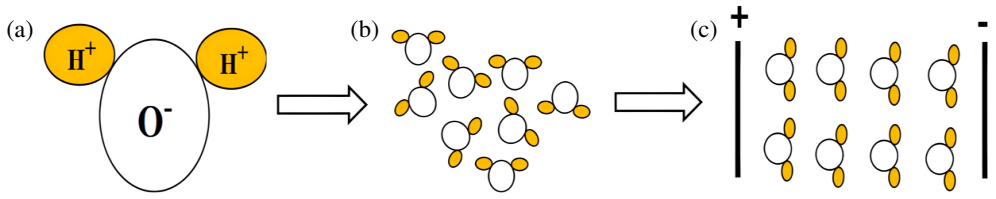

FIGURE 3. Polarization of H_2O: (a) H_2O molecule, (b) random molecule alignment, and (c) molecule alignment when a field is applied.

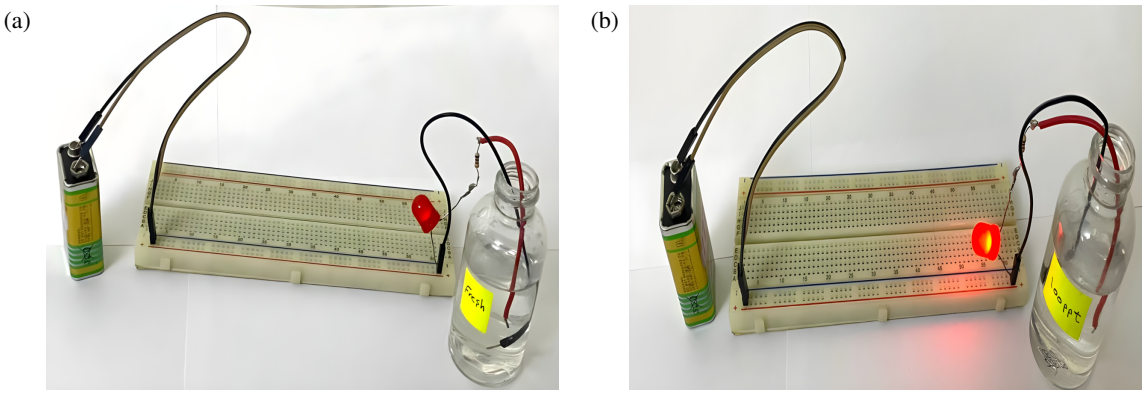

FIGURE 4. Demonstration experiment: (a) At fresh water and (b) at 100 parts per thousand.

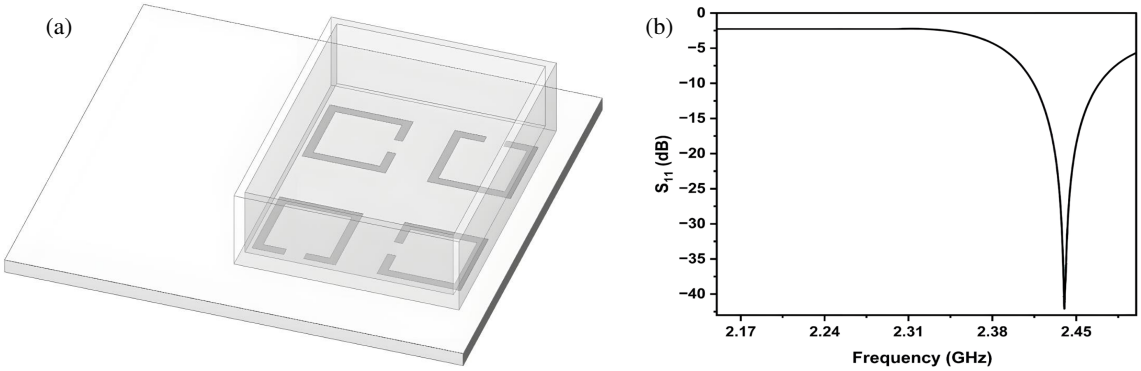

FIGURE 5. HFSS simulation for proposed sensor: (a) Final design and (b) the f_r and S_{11} values.

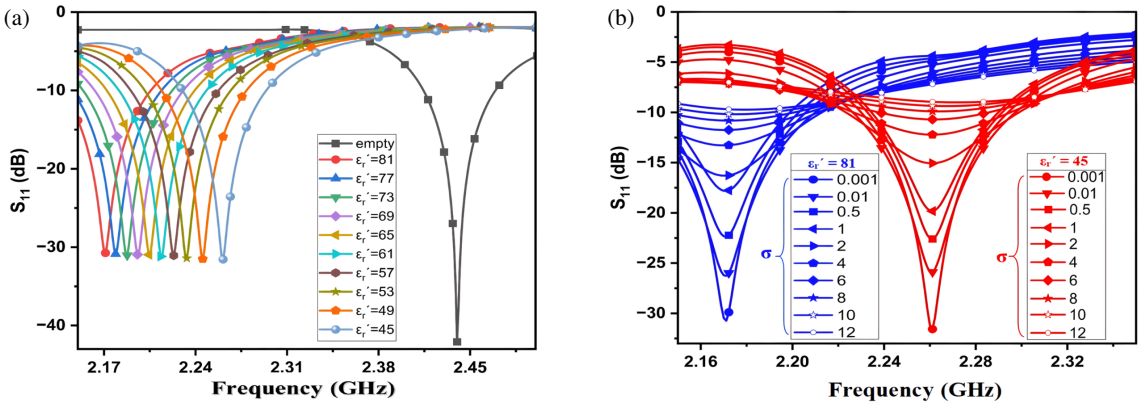

FIGURE 6. HFSS simulation for proposed sensor: (a) At constant σ and (b) at changing σ and ε_r' (81 and 45).

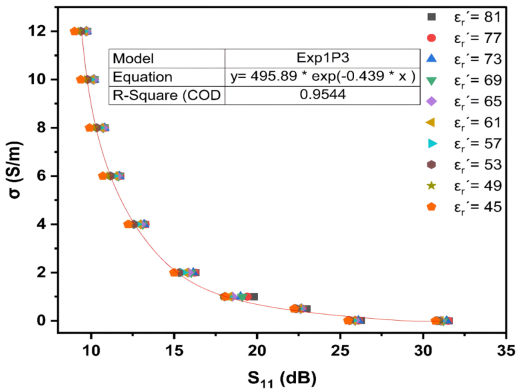

FIGURE 7. Relationship between σ and S_{11} at different ε'_r by using Origin software.

Following the determination of σ for all concentrations using the reflection coefficient, the subsequent step is to ascertain the ε'_r. As previously stated, the addition of salt to water results in the formation of dissolved ions, which reduces the number of free molecules in the water; therefore, these ions possess a lesser capacity to store electrical energy than free molecules, leading to a fall in the ε'_r and a rightward shift of the f_r (refer to Figure 6(b)). The variation in dielectric constant within the range of $81 \leq \varepsilon'_r \leq 45$, corresponding to a conductivity range of $0.001 \leq \sigma \leq 12$, is shown in Figure 8(a).

The curves in Figure 8(a) exhibit similarities at each dielectric constant; however, the distinction is in the extent of upward displacement. The numerical expressions of each curve at each dielectric constant are shown in Table 3.

TABLE 3. The numerical expression for each ε'_r.

ε'_r	Numerical expression	R^2
81	$f_r = 8\times10^{-6}\sigma^3 - 4\times10^{-5}\sigma^2 + 5\times10^{-5}\sigma + 2.1711$	0.99
77	$f_r = 1\times10^{-6}\sigma^3 - 5\times10^{-5}\sigma^2 + 5\times10^{-5}\sigma + 2.1789$	0.99
73	$f_r = 8\times10^{-6}\sigma^3 - 5\times10^{-5}\sigma^2 + 2\times10^{-4}\sigma + 2.1877$	0.98
69	$f_r = 8\times10^{-6}\sigma^3 - 7\times10^{-5}\sigma^2 + 3\times10^{-5}\sigma + 2.1956$	0.99
65	$f_r = 1\times10^{-5}\sigma^3 - 9\times10^{-5}\sigma^2 + 2\times10^{-4}\sigma + 2.2044$	0.99
61	$f_r = 7\times10^{-6}\sigma^3 - 8\times10^{-5}\sigma^2 + 3\times10^{-5}\sigma + 2.2144$	0.99
57	$f_r = 1\times10^{-6}\sigma^3 - 1\times10^{-4}\sigma^2 + 2\times10^{-4}\sigma + 2.2233$	0.99
53	$f_r = 8\times10^{-6}\sigma^3 - 1\times10^{-4}\sigma^2 + 3\times10^{-4}\sigma + 2.2332$	0.98
49	$f_r = 9\times10^{-6}\sigma^3 - 5\times10^{-5}\sigma^2 + 3\times10^{-4}\sigma + 2.2459$	0.99
45	$f_r = 8\times10^{-6}\sigma^3 - 1\times10^{-4}\sigma^2 + 3\times10^{-4}\sigma + 2.2611$	0.99

$*$ R^2 symbolizes the amount of regression.

Consequently, the equations shown in Table 3 seem similar, differing only in the constant term; hence, they will be represented by a singular standardized equation as indicated in (9).

$$f_r = 8\times10^{-6}\sigma^3 - 1\times10^{-4}\sigma^2 + 3\times10^{-4}\sigma + \text{Constant} \quad (9)$$

The constant values are then integrated with their dielectric constants, as seen in Figure 8(b).

$$\text{Constant} = 2.634 - 5.79\times10^{-3}\varepsilon'_r \quad (10)$$

Inserting Equation (10) into Equation (9) yields Equation (11).

$$\varepsilon'_r = \frac{8\times10^{-6}\sigma^3 - 1\times10^{-4}\sigma^2 + 3\times10^{-4}\sigma + 2.634 - f_r}{5.79\times10^{-3}} \quad (11)$$

The aforementioned mathematical equation was derived by a curve fitting methodology that yields a numerical expression for the proposed sensor to compute the ε'_r of the LUT, contingent upon the f_r and σ of each LUT.

Upon determining the numerical expressions for conductivity and dielectric constant, it is necessary to ascertain the loss factor, which may be readily calculated using the following relationship [43].

$$Q = \frac{\varepsilon'_r}{\varepsilon''_r} \quad (12)$$

The quality factor (Q) quantifies the ratio of stored energy to dissipated energy in an insulating medium and is inversely correlated with the attenuation of electromagnetic waves [44]. Thus, a high Q indicates less energy loss, while a low Q means increased energy loss (see to relationship 12). This is evident in highly concentrated solutions due to ionic conductivity (as shown in Figure 12). The compromise between energy storage and dissipation substantially influences the sensing system.

Utilizing relationship (12), the complex permittivity of all LUT may now be readily determined; all equations have been checked, and the results are very consistent.

6. CREATION OF SALINE SOLUTIONS AND SENSOR FABRICATION

Water salinity is quantified in ppt and is denoted by the symbol (‰), often used in oceanographic and educational contexts. It may be determined by the relationship (13) [34].

$$\text{ppt}(‰) = \frac{M_{\text{salt}}}{M_{\text{sea-water}}} \times 1000 \quad (13)$$

where M_{salt} and $M_{\text{sea-water}}$ are the mass of salt and the mass of salinity water in grams for both, respectively.

A total of 40 mL of freshwater was used for all liquid samples, with the weight of salt dissolved in grams to achieve the concentrations (0–100 ppt) shown in Table 4.

A computer numerical control (CNC) machine manufactured the proposed sensor and Teflon box, measuring $55 \times 50 \times 1.4\,\text{mm}^3$ and $35 \times 27 \times 8\,\text{mm}^3$, respectively, as shown in Figure 9(a). The proposed sensor was linked to the Sub-Miniature version A (SMA) of the Agilent Technologies E5071C Network Analyzer (Agilent Technology, Santa Rosa, USA) operating from 300 KHz to 20 GHz using a 50 Ω transmission line. f_r and S_{11} are shown on the E5071C Network Analyzer screen for varying quantities of salt (5–100 ppt) in freshwater. Figure 9(b) illustrates that the suggested sensor is equipped with a Teflon enclosure above the rings, secured with nylon self-locking mechanisms to provide stability of the readings and weight.

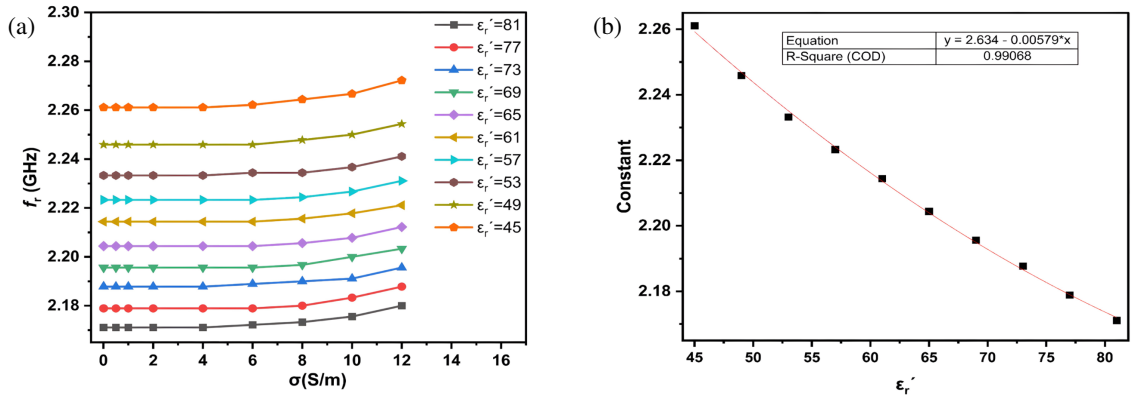

FIGURE 8. By using Origin software: (a) The variation in f_r for various conductivities and (b) a constant value with variation dielectric constant.

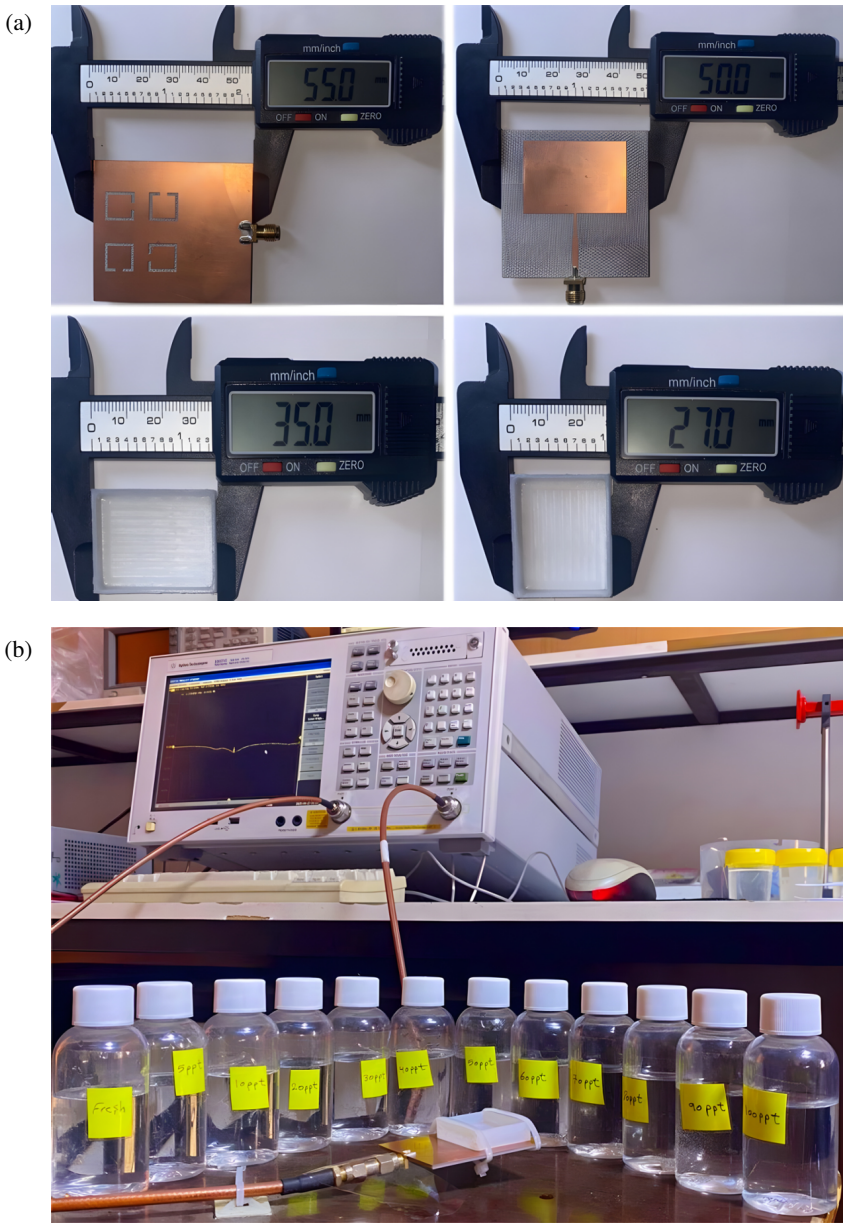

FIGURE 9. Manufacturing and experimental: (a) Dimensions of the manufactured sensor and Teflon box and (b) E5071C Network Analyzer and liquid samples with different concentrations (0–100 ppt).

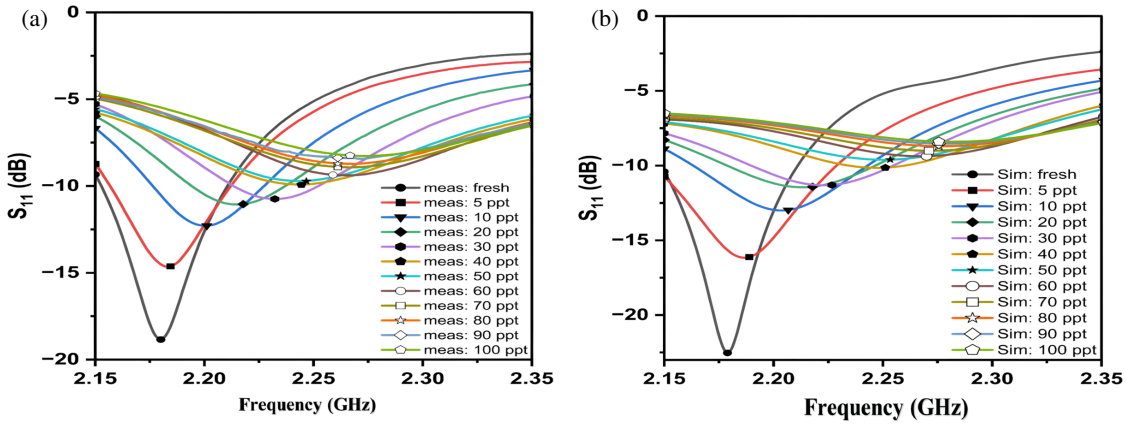

FIGURE 10. The S_{11} parameter and frequency response: (a) Measured (meas), and (b) simulated (sim).

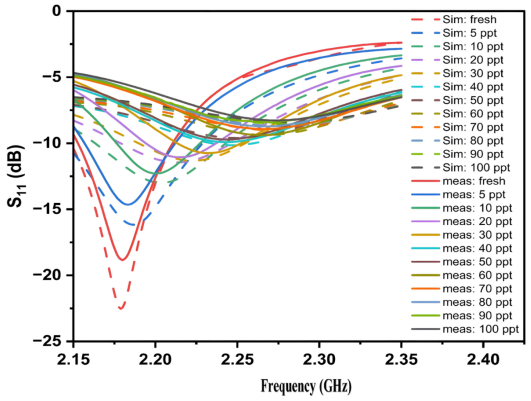

FIGURE 11. The S_{11} parameter and frequency response for both measured and simulated results.

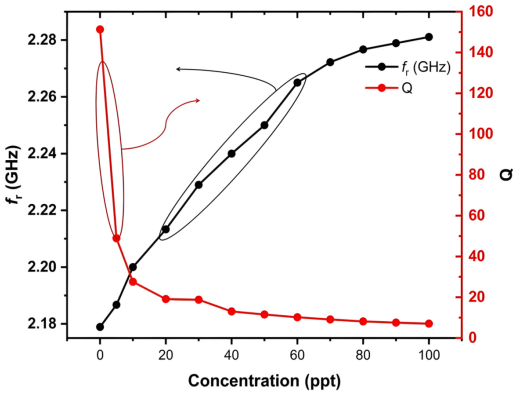

FIGURE 12. The simulated results for f_r and Q at different concentration.

TABLE 4. Concentrations of the liquid under test.

Concentrations (‰)	Mass of salt (g)
5	0.2
10	0.4
20	0.8
30	1.23
40	1.66
50	2
60	2.55
70	3
80	3.47
90	3.95
100	4.43

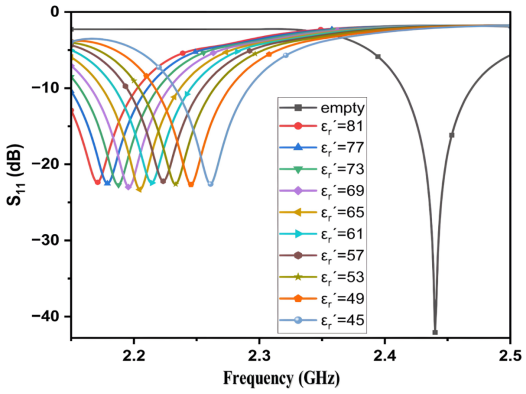

FIGURE 13. The simulated results at different ε_r' and constant σ.

7. MEASUREMENT AND SIMULATION RESULTS

Following the calibration of the E5071C network analyzer, fluids with varying concentrations (0–100 ppt) were introduced into a 2 mm high Teflon container, and S_{11} data along with f_r for each LUT were recorded. Figure 10 illustrates that the measured and simulated findings are mostly congruent.

The good matching in measured and simulated results is attributable to the accuracy of our methodology and the meticulous selection of fluid contents, alongside the lack of salt deposits in the solutions, which might induce mistakes in the results. Moreover, the appropriate securing of the axial wire and the emphasis on the elimination of dust particles or analogous pollutants enhance this uniformity.

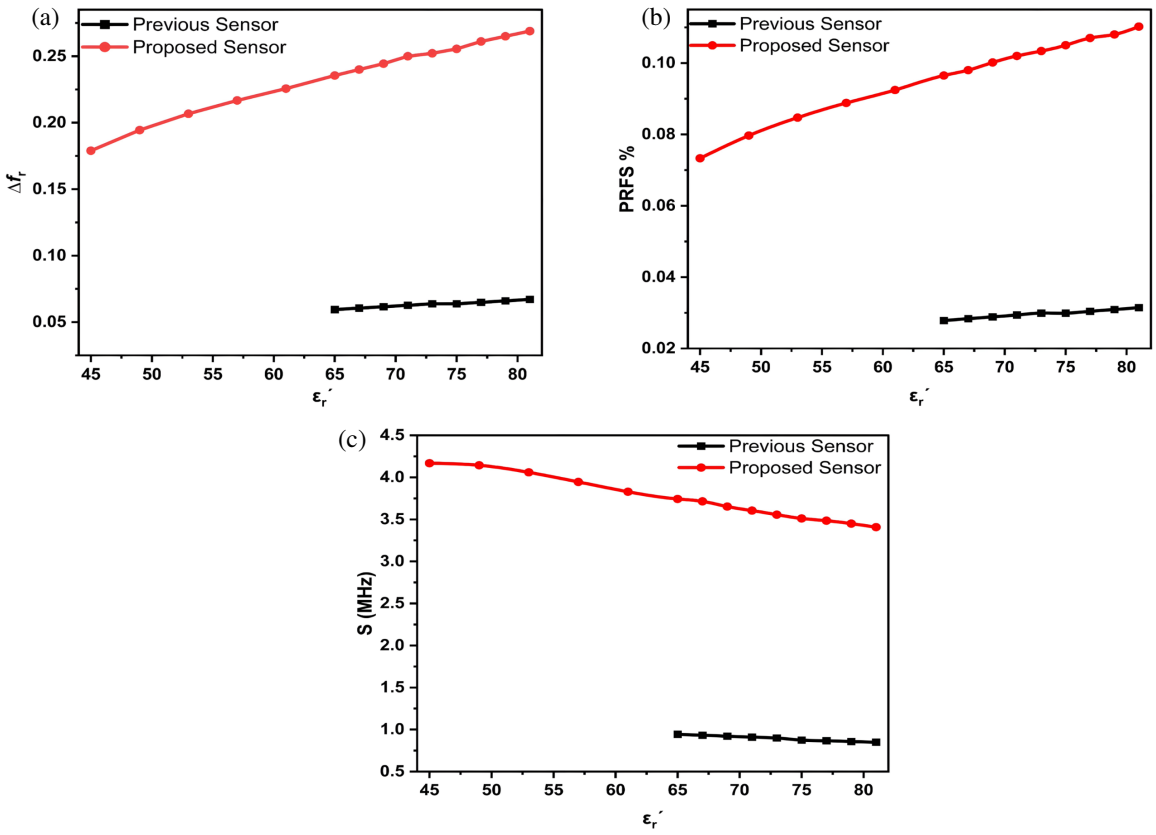

FIGURE 14. Comparison of sensitivity with [34]: (a) Δf_r, (b) PRFS, and (c) sensitivity.

To facilitate a more straightforward comparison, we will consolidate the measured and simulated results in a singular graph, as seen in Figure 11.

When examining Figure 11, one notices a slight variation between the simulated and measured results, attributed to various factors, the most significant of which is the difference between the HFSS program environment and the actual environment (including temperature, humidity, wind, etc.), along with manufacturing defects, the unreliability of the coaxial cable, and the novelty of the network analyzer.

The simulated results of the f_r and Q for LUT at varying concentrations are plotted in Figure 12.

Figure 12 demonstrates that the quality factor decreases with increasing salt concentrations (the red curve). The resonant frequencies progressively and precisely increase with higher concentrations (the black curve).

8. SENSITIVITY LEVEL COMPARISON

One can determine the sensor's sensitivity just by looking at the change in the properties of S_{11} and the resonant frequency when placing liquids of different concentrations. Figure 13 shows the shift in resonant frequency as the dielectric constant decreases from 81 to 45 in steps of 4, while conductivity remains fixed at 0.5 S/m, where the resonant frequency changed from 2.17 GHz to 2.2611 GHz.

In this section, the sensitivity of the proposed sensor is compared with the previously designed sensor [34], and for the comparison, the following equations are used [45].

$$\Delta f_r = f_{ru} - f_{rL} \tag{14}$$

$$\text{PRFS} = \frac{\Delta f_r}{f_{ru}} \times 100\% \tag{15}$$

$$S = \frac{\Delta f_r}{\varepsilon'_{ru} - \varepsilon'_{rL}} \tag{16}$$

where f_{ru} and f_{rL} are the resonance frequencies at unload and load conditions, respectively; ε'_{ru} and ε'_{rL} are the dielectric constants at unload and load conditions, respectively; S is sensitivity; and PRFS is the perfect relation frequency shift.

Figure 14 illustrates the resonant frequency, PRFS, and sensitivity of both the proposed sensor and the previous sensor. It is evident that the proposed sensor exhibits a significantly greater shift in resonant frequency than the previous sensor when the dielectric constant is altered, as depicted in Figure 14(a). The PRFS denotes the ideal alteration in resonance frequency resulting from a variation in the dielectric constant, since this shift is essential for enhancing sensitivity and precision in sensing applications. Figure 14(b) illustrates that the suggested strategy is superior. Sensitivity refers to the extent of responsiveness of the resonant frequency to minimal changes in dielectric characteristics, often quantified in gigahertz for dielectric constants ranging from 1 to 10. In liquids with very high dielectric constants, such as water, sensitivity diminishes inversely, as seen in Equation (16). Consequently, measuring it in megahertz is better suited for liquids with elevated dielectric constants. Figure

TABLE 5. Comparison of the proposed sensor with existing works in the literature.

Ref	Method	f_r GH	LUTs	The flaws
[11]	Circular ring monopole	2.4	Solutions (sugar, salt)	-This approach is elevated due to the need for conductive yarn and an embroidery machine. -It must be cleaned and allowed to dry after each measurement.
[13]	Stepped structure	5.3 7.4 8.6	various water (Distilled, Rain, Pool, Sea, R.O.)	-Water immersion leads to the degradation of critical components of the sensor. -The frequency shift is minimal as concentrations rise.
[22]	Hexagonal SRR	2.9 5 11.2	PH of water	-Two microstrip patch antennas are required. -Large amount of liquid Approximately 350 mL
[29]	notches and defected ground plane	3.5 6.5 8.5 9.7	Salt in various water (Distilled, R.O., and Raw)	-The detection of salt in water relies only on the alteration of the reflection coefficient. -Water immersion leads to the degradation of critical components of the sensor.
[46]	CSRR	2.1	Ethanol concentration in water	-The introduction of fluid into the microfluidic channel may generate air bubbles that are difficult to remove, so compromising the precision of the results. -The microfluidic channel is difficult to dry after rinsing with distilled water
[47]	Crescent-shaped patch and slotted partial ground	3.2 8.7 11.6 14.5	Salt and sugar solution	-Water immersion leads to the degradation of critical components of the sensor. -The presence of sediment in the samples causes inaccurate results.

R.O. refers to reverse osmosis water.

14(c) illustrates that the proposed sensor exhibits a sensitivity 3.96 to 4 times superior to that of the previous sensor within dielectric constants ranging from 65 to 81. Furthermore, we observe that the sensor's sensitivity escalates with elevated salt concentrations, signifying its suitability for the use at high concentrations.

9. COMPARISON OF THE PROPOSED SENSOR WITH EXISTING WORKS IN THE LITERATURE

The proposed sensor design using SC-SRRs methodology shows significant progress compared to previous research, as shown in Table 5. Several key features are highlighted, including: no contact between liquid samples and the sensor, no deposits in the LUTs, the smallest required amount of LUT, cost-effectiveness, high-frequency conversion, and higher sensitivity.

10. CONCLUSION

This work proposes a sensor that includes four SC-SRRs etched in the ground plane for microwave characterization of saline solutions. When the liquid being tested is introduced, the resonant frequency, reflection coefficient, and quality factor change because of the effects of different salt concentrations (0–100 ppt), resulting in a shift of 104.4 MHz in the resonance frequency. The proposed sensor has excellent sensitivity, calculated in megahertz units, due to the high permittivity of water compared to other liquids. Also the measured and simulated results showed excellent agreement due to the precision of our work and the use of accurate and correct method. Additionally, numerical expressions were created to determine both the conductivity and dielectric constant for each LUT, and they were verified with good results. Due to the high performance of the proposed sensor, we believe that it can be applied to other liquids. In future work, different concentrations of certain fluids such as blood, urea, and saliva will be tested.

ACKNOWLEDGEMENT

This work was supported by the Al-Mustansiriyah University, College of Engineering.

REFERENCES

[1] Garg, R., *Microstrip Antenna Design Handbook*, Artech House, Boston, MA, USA, 2001.

[2] Ahmed, S., A. A. Albehadili, Z. H. Mohammed, Z. A. A. Hassain, M. Al-Saadi, and M. Chandra, "Circularly polarized hexagonal microstrip antenna loaded with slot and complementary split ring resonator," *Journal of Engineering and Sustainable Development*, Vol. 28, No. 6, 745–753, 2024.

[3] Al-Gertany, K. and Q. Hadi, "Reconfigurable compact wideband quad-port antennas based on a varactor diode for sub-6 GHz 5G communications," *Progress In Electromagnetics Research C*,

Vol. 145, 91–100, 2024.

[4] Bennioui, F.-Z., A. Khabba, K. A. Bouslam, L. Wakrim, S. Ibnyaich, A. Zeroual, Z. Zakaria, and A. J. A. Al-Gburi, "Genetic algorithm optimization of a wideband rectangular patch antenna with an asymmetric U-slot and partial ground for Ku-band satellite communication," *Progress In Electromagnetics Research M*, Vol. 133, 51–60, 2025.

[5] Indharapu, S. S., A. N. Caruso, T. D. Fields, and K. C. Durbhakula, "Machine learning-based optimization of hexagon-shaped fractal antenna for ultra-wideband communications," *Progress In Electromagnetics Research C*, Vol. 143, 121–129, 2024.

[6] Kareem, Q. H., L. W. Abdullah, R. A. Shihab, F. A. J. Al-Hasani, and S. N. Abdullah, "Optimize the performance of reconfigurable antenna based on laser treatment for sub-6 GHz applications," *Progress In Electromagnetics Research Letters*, Vol. 123, 95–103, 2025.

[7] Kareem, Q. H. and M. J. Farhan, "Miniaturized quad-port UWB-MIMO antenna with band-notched characteristics at 5 GHz," *Progress In Electromagnetics Research C*, Vol. 118, 263–275, 2022.

[8] Prottoy, S. S., M. M. Rana, M. A. Islam, M. Arifuzzaman, and N. Alam, "Inverse S-shaped meander line antenna loaded with slotted parasitic patch and defected ground for internet of things (IoT) applications," *Progress In Electromagnetics Research C*, Vol. 154, 31–38, 2025.

[9] Malik, N. A., P. Sant, T. Ajmal, and M. Ur-Rehman, "Implantable antennas for bio-medical applications," *IEEE Journal of Electromagnetics, RF and Microwaves in Medicine and Biology*, Vol. 5, No. 1, 84–96, 2021.

[10] Wang, W., X.-W. Xuan, W.-Y. Zhao, and H.-K. Nie, "An implantable antenna sensor for medical applications," *IEEE Sensors Journal*, Vol. 21, No. 13, 14 035–14 042, 2021.

[11] El Gharbi, M., M. Martinez-Estrada, R. Fernández-García, and I. Gil, "Determination of salinity and sugar concentration by means of a circular-ring monopole textile antenna-based sensor," *IEEE Sensors Journal*, Vol. 21, No. 21, 23 751–23 760, 2021.

[12] Lee, K., A. Hassan, C. H. Lee, and J. Bae, "Microstrip patch sensor for salinity determination," *Sensors*, Vol. 17, No. 12, 2941, 2017.

[13] Logeswaran, J. and R. B. Rani, "UWB antenna as a sensor for the analysis of dissolved particles and water quality," *Progress In Electromagnetics Research Letters*, Vol. 106, 31–39, 2022.

[14] Costanzo, S., A. Cuccaro, A. Dell'Aversano, G. Buonanno, and R. Solimene, "Microwave biomedical sensors with stable response: Basic idea and preliminary numerical assessments for blood glucose monitoring," *IEEE Access*, Vol. 11, 99 058–99 069, 2023.

[15] Kandwal, A., J. Li, T. Igbe, Y. Liu, R. Das, B. K. Kanaujia, and Z. Nie, "Young's double slit method-based higher order mode surface plasmon microwave antenna sensor: Modeling, measurements, and application," *IEEE Transactions on Instrumentation and Measurement*, Vol. 71, 1–11, 2022.

[16] Raj, S., S. Tripathi, G. Upadhyay, S. S. Tripathi, and V. S. Tripathi, "An electromagnetic band gap-based complementary split ring resonator loaded patch antenna for glucose level measurement," *IEEE Sensors Journal*, Vol. 21, No. 20, 22 679–22 687, 2021.

[17] Sindhuja, S. and E. Kanniga, "Flexible antenna sensor in thumb spica splint for noninvasive monitoring of fluctuating blood glucose levels," *IEEE Sensors Journal*, Vol. 23, No. 1, 544–551, 2023.

[18] Sanders, J. W., J. Yao, and H. Huang, "Microstrip patch antenna temperature sensor," *IEEE Sensors Journal*, Vol. 15, No. 9, 5312–5319, 2015.

[19] Zhang, L., S. Su, F. Xu, T. Ren, and J. Xiong, "High sensitivity SIW-CSRR temperature sensor based on microwave scattering," *IEEE Sensors Journal*, Vol. 23, No. 13, 13 900–13 908, 2023.

[20] Javanbakht, N., G. Xiao, and R. E. Amaya, "A comprehensive review of portable microwave sensors for grains and mineral materials moisture content monitoring," *IEEE Access*, Vol. 9, 120 176–120 184, 2021.

[21] Zeng, Z., L. Huang, L. Dang, L. Sai, Q. Chang, and W. Shi, "RSSI evaluation model for quantitative power-oriented sensing using an omnidirectional antenna sensor," *IEEE Sensors Letters*, Vol. 2, No. 1, 1–4, 2018.

[22] Islam, M. T., F. B. Ashraf, T. Alam, N. Misran, and K. B. Mat, "A compact ultrawideband antenna based on hexagonal split-ring resonator for pH sensor application," *Sensors*, Vol. 18, No. 9, 2959, 2018.

[23] Halmshaw, R., "Basic properties of ionizing radiations," in *Industrial Radiology: Theory and Practice*, 9–32, Springer, 1995.

[24] Zografopoulos, D. C., A. Ferraro, and R. Beccherelli, "Liquid-crystal high-frequency microwave technology: Materials and characterization," *Advanced Materials Technologies*, Vol. 4, No. 2, 1800447, 2019.

[25] Alozie, E., A. Musa, N. Faruk, A. L. Imoize, A. Abdulkarim, A. D. Usman, Y. O. Imam-Fulani, K. S. Adewole, A. A. Oloyede, O. A. Sowande, S. Garba, B. A. Baba, Y. A. Adediran, and L. S. Taura, "A review of dust-induced electromagnetic waves scattering theories and models for 5G and beyond wireless communication systems," *Scientific African*, Vol. 21, e01816, 2023.

[26] Yan, D., Y. Yang, Y. Hong, T. Liang, Z. Yao, X. Chen, and J. Xiong, "Low-cost wireless temperature measurement: Design, manufacture, and testing of a pcb-based wireless passive temperature sensor," *Sensors*, Vol. 18, No. 2, 532, 2018.

[27] Kou, H., Q. Tan, L. Zhang, H. Dong, J. Xiong, and W. Zhang, "Highly sensitive air-filled substrate integrated waveguide resonator integrated wireless passive slot-antenna for confined environmental detection," *IEEE Sensors Journal*, Vol. 19, No. 21, 10 027–10 033, 2019.

[28] Iqbal, A., A. Smida, O. A. Saraereh, Q. H. Alsafasfeh, N. K. Mallat, and B. M. Lee, "Cylindrical dielectric resonator antenna-based sensors for liquid chemical detection," *Sensors*, Vol. 19, No. 5, 1200, 2019.

[29] Joseph, C. V., S. Ramesh, Z. Z. Abidin, S. A. Qureshi, S. Chitra, E. Saranya, M. Josephine, and G. Sneha, "Planar edged UWB antenna for water quality measurement," *Progress In Electromagnetics Research C*, Vol. 130, 83–93, 2023.

[30] Eldamak, A. R. and E. C. Fear, "Conformal and disposable antenna-based sensor for non-invasive sweat monitoring," *Sensors*, Vol. 18, No. 12, 4088, 2018.

[31] Tang, L., F. Xie, and Q. Li, "A phase shift-based and quadrant-distinguishable passive microstrip antenna sensor for metal crack detection," *IEEE Sensors Journal*, Vol. 24, No. 6, 7796–7806, 2024.

[32] Withayachumnankul, W., K. Jaruwongrungsee, A. Tuantranont, C. Fumeaux, and D. Abbott, "Metamaterial-based microfluidic sensor for dielectric characterization," *Sensors and Actuators A: Physical*, Vol. 189, 233–237, 2013.

[33] Ansari, M. A. H., A. K. Jha, and M. J. Akhtar, "Permittivity measurement of common solvents using the CSRR based sensor," in *2015 IEEE International Symposium on Antennas and Propagation & USNC/URSI National Radio Science Meeting*, 1199–1200, Vancouver, BC, Canada, Jul. 2015.

[34] Jasim, H., S. Ahmed, I. A. Mocanu, and A. A. Al-Behadili, "Microstrip patch sensor for characterizing saline solution based on complimentary split-ring resonators (SC-SRRs)," *Sensors*, Vol. 25, No. 7, 2319, 2025.

[35] Javed, A., A. Arif, M. Zubair, M. Q. Mehmood, and K. Riaz, "A low-cost multiple complementary split-ring resonator-based microwave sensor for contactless dielectric characterization of liquids," *IEEE Sensors Journal*, Vol. 20, No. 19, 11 326–11 334, 2020.

[36] Abdulsattar, R. K., M. T. S. Al-Kaltakchi, I. A. Mocanu, A. A. Al-Behadili, and Z. A. A. Hassain, "Study on sensing urine concentrations in water using a microwave sensor based on hilbert structure," *Sensors*, Vol. 24, No. 11, 3528, 2024.

[37] Anwer, A. I., Z. A. A. Hassain, and T. A. Elwi, "A fractal minkowski design for microwave sensing applications," *Journal of Engineering and Sustainable Development*, Vol. 26, No. 5, 78–83, 2022.

[38] Balanis, C. A., *Antenna Theory: Analysis and Design*, 811–856, John Wiley & Sons, NJ, USA, 2016.

[39] Reddy, A. C., "Characterization of mechanical behavior of nylon/teflon nano particulate composites," *International Journal of Advanced Research*, Vol. 3, No. 5, 1241–1246, 2015.

[40] Agilent Technologies, Inc., "Agilent basics of measuring the dielectric properties of materials," Application Note, 1–34, 2006.

[41] Nörtemann, K., J. Hilland, and U. Kaatze, "Dielectric properties of aqueous NaCl solutions at microwave frequencies," *The Journal of Physical Chemistry A*, Vol. 101, No. 37, 6864–6869, 1997.

[42] Schmitt, R., *Electromagnetics Explained: A Handbook for Wireless/RF, EMC, and High-Speed Electronics*, Newnes, 2002.

[43] Al-Behadili, A. A., I. A. Mocanu, N. Codreanu, and M. Pantazica, "Modified split ring resonators sensor for accurate complex permittivity measurements of solid dielectrics," *Sensors*, Vol. 20, No. 23, 6855, 2020.

[44] Nel, B. A. P., A. K. Skrivervik, and M. Gustafsson, "Q-factor bounds for microstrip patch antennas," *IEEE Transactions on Antennas and Propagation*, Vol. 71, No. 4, 3430–3440, 2023.

[45] Yeo, J. and J.-I. Lee, "Meander-line slot-loaded high-sensitivity microstrip patch sensor antenna for relative permittivity measurement," *Sensors*, Vol. 19, No. 21, 4660, 2019.

[46] Salim, A. and S. Lim, "Complementary split-ring resonator-loaded microfluidic ethanol chemical sensor," *Sensors*, Vol. 16, No. 11, 1802, 2016.

[47] Islam, M. T., M. N. Rahman, M. S. J. Singh, and M. Samsuzzaman, "Detection of salt and sugar contents in water on the basis of dielectric properties using microstrip antenna-based sensor," *IEEE Access*, Vol. 6, 4118–4126, 2018.